

This item is the archived peer-reviewed author-version of:

Mono- and multilayer silicene-type honeycomb lattices by oriented attachment of PbSe nanocrystals : synthesis, structural characterization, and analysis of the disorder

Reference:

Peters Joep L., Altantzis Thomas, Lobato Hoyos Ivan Pedro, Alimoradi Jazi Maryam, van Overbeek Carlo, Bals Sara, Vanmaekelbergh Daniel, Buhbut Sinai Sophia.-
Mono- and multilayer silicene-type honeycomb lattices by oriented attachment of PbSe nanocrystals : synthesis, structural characterization, and analysis of the disorder
Chemistry of materials - ISSN 0897-4756 - 30:14(2018), p. 4831-4837
Full text (Publisher's DOI): <https://doi.org/10.1021/ACS.CHEMMATER.8B02178>
To cite this reference: <https://hdl.handle.net/10067/1529970151162165141>

Mono- and Multilayer Silicene-Type Honeycomb Lattices by Oriented Attachment of PbSe Nanocrystals: Synthesis, Structural Characterization, and Analysis of the Disorder.

Joep L. Peters,[†] Thomas Altantzis,[‡] Ivan Lobato,[‡] Maryam Alimoradi Jazi,[†] Carlo van Overbeek,[†] Sara Bals,[‡] Daniel Vanmaekelbergh^{†*}, Sophia Buhbut Sinai,[†]

[†] Condensed Matter and Interfaces, Debye Institute for Nanomaterials Science, Utrecht University, P.O. Box 80000, 3508 TA Utrecht, The Netherlands

[‡] EMAT, University of Antwerp, Groenenborgerlaan 171, B-2020 Antwerp, Belgium

* Corresponding author

KEYWORDS (Word Style “BG_Keywords”): interfacial self-assembly, oriented attachment, tomography, structural disorder

ABSTRACT: Nanocrystal (NC) solids are commonly prepared from non-polar organic suspensions, with preservation of the original capping. On the other hand, NC superstructures with a direct crystalline connection between the NCs have been reported too. Here, we present large-scale uniform superstructures of attached PbSe NCs with a silicene-type honeycomb

geometry, resulting from solvent evaporation under nearly reversible conditions. We also prepared multilayered silicene honeycomb structures by using larger amounts of PbSe NCs. We show that the two-dimensional silicene superstructures can be seen as a crystallographic slice from a 3-D simple cubic structure. We describe the disorder in the silicene lattices in terms of the nanocrystals position and their atomic alignment. The silicene honeycomb sheets are large enough to be used in transistors and opto-electronic devices.

TEXT:

Thin solid films of semiconductor nanocrystals hold promise for several opto-electronic applications, such as LEDs^{1,2}, photo-detectors³ and solar cells^{4,5,6}. Commonly, non-polar suspensions are used in which the nanocrystals are sterically stabilised by long organic capping molecules, and this capping is preserved in the NC solids. The resulting poor electronic coupling between the nanocrystals has been a major concern in the last years. Considerable progress has been made by smart surface chemistry, either on the level of the dispersed NCs^{7,8}, or as a post treatment on the nanocrystals present in the solid^{9,10,11}.

In recent years, much effort has been put in the formation of nanocrystal solids in which the nanocrystals are epitaxially connected via specific facets^{12,13,14,15,16}. Since this attachment is crystallographic in nature, atomically coherent structures are fabricated with one (rods)^{12,17,18}, two (sheets)^{12,13,16,19}, or even three extended dimensions²⁰. Once the process of epitaxial attachment is under control, it might form a bottom-up pathway for semiconductor structures, such as wires and quantum wells, complementary to the established but precious gas-phase methods. Moreover, it was shown recently that oriented attachment may result in two-dimensional structures with a superimposed square or honeycomb geometry¹². This is due to the specific truncated cubic shape of the PbSe nanocrystals and the precise attachment via (100) facets only¹⁶. It has been theoretically predicted that the in-plane nanogeometry should strongly influence the semiconductor band structure^{21,22,23,24}. The honeycomb structure for instance, with its similarity to graphene and silicene, results in Dirac-type valence and conduction bands with massless holes and electrons²³. To bring this scientific field forward and push it towards technological innovations, the chemical methodology of self-assembly and oriented attachment

should be improved considerably for enhanced reproducibility, larger scale crystallographic domains, and full control of the nanogeometry.

Here, we show how to prepare silicene-type honeycomb structures from PbSe nanocrystals with lateral dimensions in the 10 - 100 μm range in a reproducible manner. The process of NC self-assembly was changed such that it could occur under nearly reversible conditions. Solvent evaporation occurred under a gas atmosphere that was nearly saturated with the solvent, such that the entire process time slowed down to 16 hours. These nearly reversible conditions for the 2-D nanocrystal phases that precede the oriented NC attachment resulted in reproducible formation of large-scale 2-D silicene honeycomb domains. Moreover, by casting more PbSe nanocrystal building blocks on the liquid substrate, we can extend the silicene structures in the third (vertical) dimension. We performed high angle annular dark-field scanning transmission electron microscopy (HAADF-STEM) tomography experiments and acquired selected area electron diffraction (SAED) patterns along different tilt angles revealing the interrelation between all PbSe NC structures observed so far: The two-dimensional silicene superstructure with three connections per NC, and the planar square structures with four connections per NC can be considered as crystallographic slices taken from the 3-D simple cubic superlattice. Finally, we studied the disorder on the level of the nanocrystal positions in the silicene lattice, and on the level of atomic plane misalignment due to imperfect epitaxy.

Methodology: There are two main methods to induce oriented attachment between Pb-chalcogenide NCs. The first method uses amines to L-type displace the Z-type $\text{Pb}(\text{oleate})_2$ ligand and thereby induce attachment between (100) facets of the NCs^{13,14,20,25}. In the second method, a Pb-chalcogenide NC suspension in a non-polar solvent is casted on ethylene glycol [EG], functioning as a liquid substrate. Solvent evaporation results in the formation of 2-D sheets that

consists of domains with crystals attached in a linear fashion, a square geometry and a honeycomb geometry¹².

Our group has used the second method and has put the reaction system directly under nitrogen atmosphere in a glove box, resulting in relatively fast solvent evaporation and formation of a solid superstructure (typical process times were 20-40 minutes). We obtained sheets of a NC monolayer thickness in which the NCs were epitaxially attached; the sheets showed domains with a square and/or honeycomb geometry. The method of fast evaporation has, however, not been optimized and lacks the reproducibility required for technological innovation: The relative amounts of square, and honeycomb structures varied considerably with the experiment, and the size of the superstructure domains was rather small ($< 1 \mu\text{m}$), and also varied from experiment to experiment.

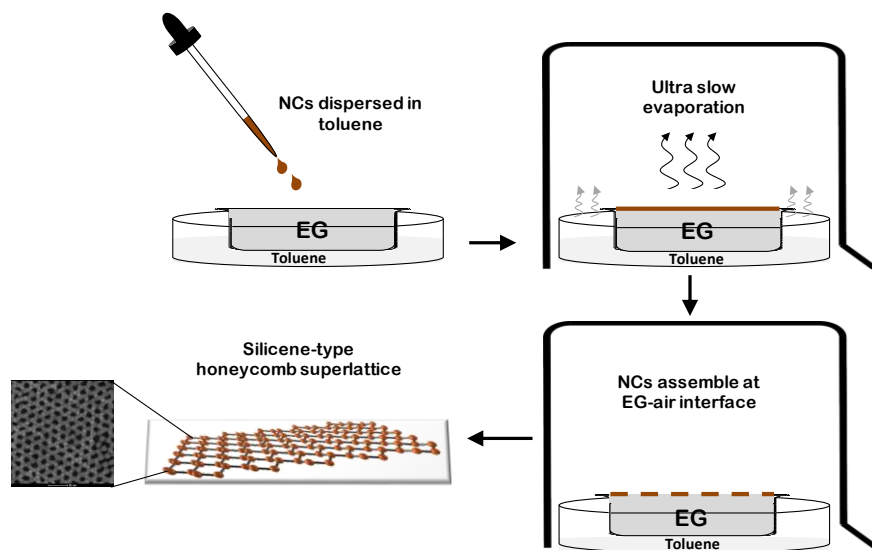


Figure 1. Schematic representation of the experimental setup and methodology. In the first step a 6.5 mL petri dish is filled with ethylene glycol serving as a liquid substrate. This dish is then placed in a larger petri dish containing 2 mL toluene. A PbSe NC suspension with a controlled amount of NCs is drop casted on the EG substrate and a beaker is placed on top to

slow down the evaporation. Solvent evaporation and superlattice formation takes 16 hours. The NC sheet that is formed on the liquid substrate is transferred onto a desired substrate or TEM grid. The entire handling is performed in a glovebox with less than 0.1 ppm oxygen.

Here, we show how we optimized the synthesis of honeycomb superstructures by choosing for very slow process conditions, i.e. very slow evaporation of the toluene solvent from the nanocrystal dispersion (see Figure 1), which is under a gas atmosphere nearly saturated with toluene. A petri dish is fully filled with EG creating a flat liquid surface. This petri dish is then placed in a second larger petri dish filled with 2 mL of toluene. A PbSe NC dispersion in toluene with a controlled amount of NCs (5 - 6.3 nm in size) is drop casted on top of the EG liquid substrate and both petri dishes are covered with a beaker. This entire handling is performed in a glovebox with <0.1 ppm oxygen. Due to the presence of a toluene liquid phase in this set-up, the gas atmosphere above the NC dispersion has a constant and large toluene partial pressure; this slows down the process of solvent evaporation enormously. We collected the NC sheets typically after 16 hours of process time.

Two-dimensional silicene sheets as the dominant phase: Figure 2 shows a typical picture of the samples obtained with the method explained above when the amount of NCs drop casted was chosen to form a monolayer system. The optical microscope image shows large dark blue colored domains surrounded by a paler background. The dark-blue domains have dimensions in the 10 - 100 μm range and boundaries with a nearly minimized contact line (see Figure S1 for more examples). Here, solvent evaporation must be slower than the diffusion of NCs in a lateral plane and nanocrystals can find positions of minimal energy^{26,27,28}. It is reasonable to assume that all processes that precede oriented attachment, i.e. the formation of 2-D NC structures with a

specific geometry and nanocrystal orientation induced by desorption of the capping ligands from the (100) facets have time to occur under natural reaction conditions, i.e. without transport limitations. We remark that faster solvent evaporation results in irregular drying patterns, coffee stains^{29,30,31,32,33,34}, or even fractal structures^{28,35}. For convenience, we have repeated the experiments under fast solvent evaporation and observed coffee stain structures and fractal domains consisting of linear, square and honeycomb superstructures (Figures S2 and S3).

By a more detailed inspection of the transmission electron microscopy (TEM) images in Figure 2 it becomes clear that the darker structures have a honeycomb geometry, while the lighter regions consist of a monolayer film of PbSe NCs attached in linear and square structures. The darker blue regions in the optical images must correspond to the darker regions on the TEM images, and indicate a higher NC density. Electron diffraction shows that in the honeycomb domains all the nanocrystals are aligned with the $\langle 111 \rangle$ direction perpendicular to the plane, and that the (100) planes are also aligned. This indicates that the PbSe NCs in these honeycomb structures are epitaxially connected. Since the TEM images in Figure 2 only correspond to 2D projections, electron tomography was applied to obtain conclusive evidence in 3D (Figure 3e). Similar honeycomb structures have been previously reported, and identified to have a buckled silicene-like geometry, 2 NC monolayers (2ML) in thickness¹⁶. We can conclude that slow solvent evaporation results in a substantial improvement with respect to the previous fast procedure, both with regard to the reproducibility and specificity of the final product (i.e. the desired honeycomb lattice) and the lateral dimensions of the domains, now in the 100 μm range instead of 0.1 - 5 μm .

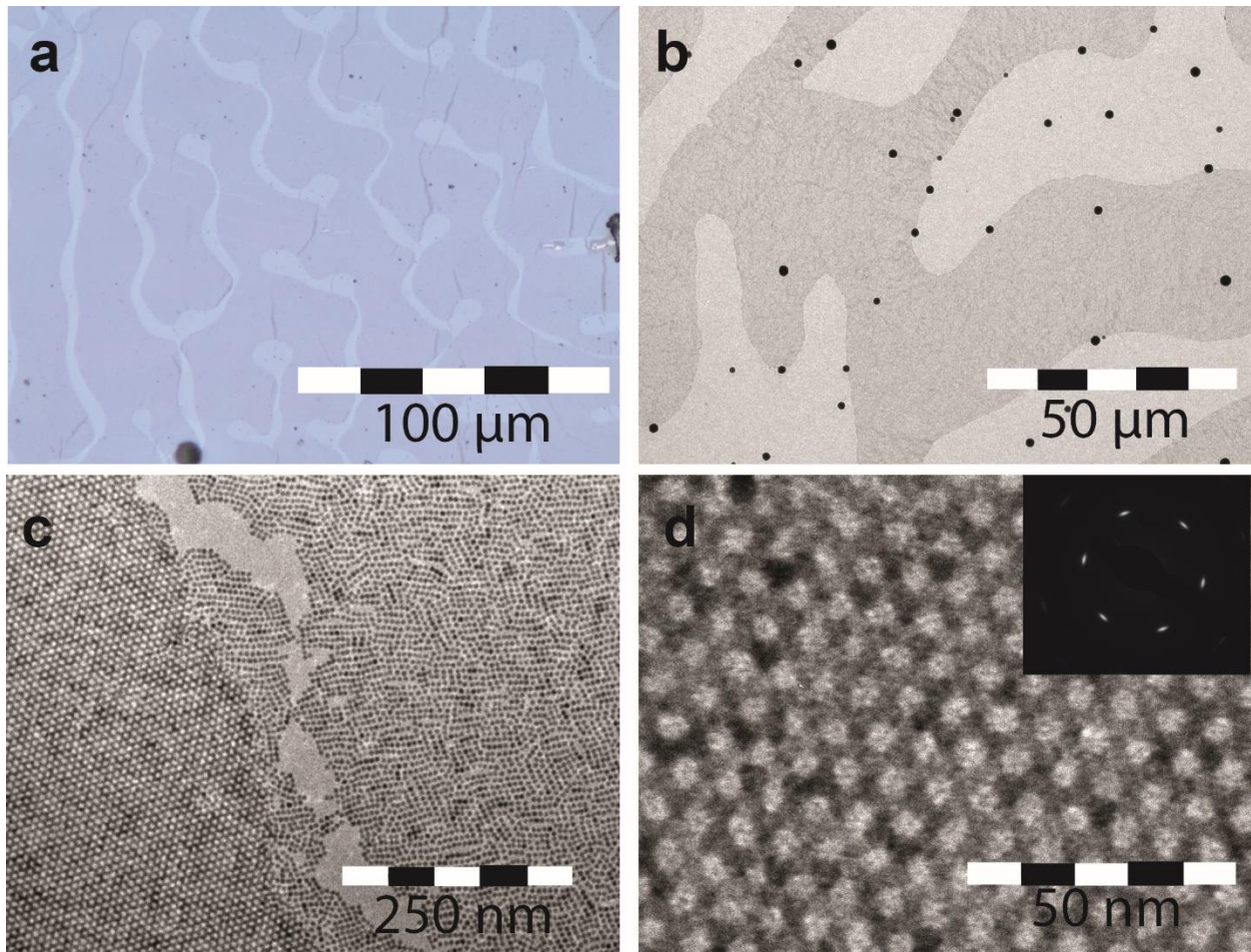


Figure 2. Global and zoomed in images of the PbSe sheets formed by slow processing. (a) optical microscope image showing large uniform domains ($> 10 \mu\text{m}$, dark blue) surrounded by thinner sheets (pale blue). (b) Low magnification TEM image showing similar uniform domains (dark gray) surrounded by domains with a lower density of nanocrystals. (c) A zoomed-in TEM image showing that the denser domains have a honeycomb periodicity, while the paler regions consist of square or linear structures with a thickness of a nanocrystal monolayer. (d) High magnification TEM image of the honeycomb structure; the inset shows a SAED pattern with six spots on the 220 ring, proving that the nanocrystals are aligned with their $\langle 111 \rangle$ crystallographic axis upwards and also aligned in plane.

Multilayer silicene structures: When we increased the amount of NCs casted on the EG, solid films thicker than 1-2 NC ML should necessarily be formed. The question is then if the nanocrystals are also epitaxially connected, and what type of NC solids form? A typical result is presented and analyzed in Figure 3. Figure 3a shows a multi-layer structure with a sequence of terraces, very similar to what can be found on the surface of atomic solids. The multilayer domains can be tens of micrometers in the lateral dimensions and up to 10 layers in the vertical dimension. Such domains are surrounded by sheets of buckled silicene-like structures. SAED acquired from each of the terraces shows that the NCs are similarly oriented, indicating that the entire superstructure with all its terraces is in fact a single crystal with buckled silicene geometry. This is corroborated by the HAADF-STEM image of Figure 3c that shows the step between a visible silicene honeycomb (the 2 ML layer structure) and a 3 ML structure. By changing the angle of the sample with respect to the electron beam it is shown that the nanocrystals are connected via epitaxial necks, in the 2ML structure and in the 3ML superstructure as well. This is also shown for the region between the 3ML and 4ML in figure S4. Electron tomography series were acquired of this specific region and a 3D visualisation of the manually segmented reconstruction is presented in Figure 3e. From the reconstruction, the number of layers can be determined as well as their 3D stacking along the axis perpendicular to the substrate. Moreover, a grain boundary was observed between a domain with 3 and one with 4 layers of NCs. Furthermore, it can be seen that each of the bottom NCs (purple) is surrounded in a trigonal way by three NCs of the second layer. Similar, the NCs of the second layer (green) are surrounded by 3 NCs of the third layer (blue), meaning that an ABC order is present in the vertical direction. In the other grain, NCs of the 4th layer are above those of the first layer, i.e. an ABCA order. This is in complete agreement with a multilayered superstructure with silicene-type geometry. The

idealized schemes in Figure 3f show the structures consisting of 3 and 4 layers of NCs. The same analysis is also performed for the transition region between two domains with 4 and 5 layers of NCs, shown in figure S5. For the structure that consists of 5 layers of NCs we observe an overall ABCAB stacking. This reveals that our multilayered silicene structures are, in fact, a part of a simple cubic NC superstructure. This also means that the buckled 2ML silicene honeycomb structure can be considered as a crystallographic slice taken from a simple cubic structure. In the 2ML silicene structure, the NCs have three neighbors connected via NC(100)/(100)NC epitaxy, with bonding angles of 90 degrees. We would like to remark here that atomic crystals with simple cubic structure are extremely rare limited to special elements, such as Polonium. While the atomic volume fraction of such a Po crystal is low (52%), it is even lower in the NC superstructure (32 %), due to the necks between the NCs.

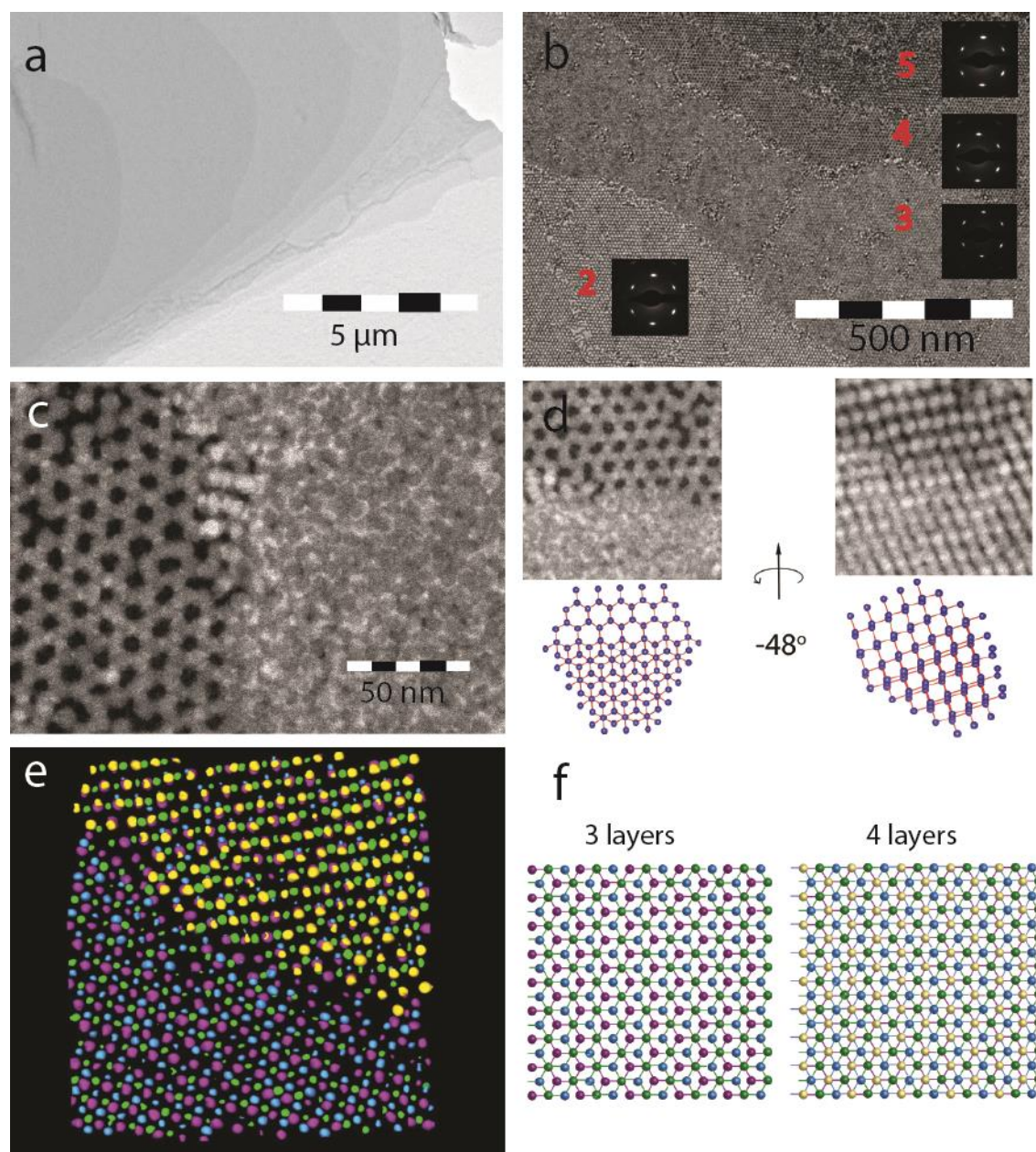


Figure 3. Structural analysis of multi-layered superstructures formed under nearly reversible conditions. (a) TEM image showing a multilayered domain, terraces indicate the number of NCs in the vertical direction. (b) TEM image of thinnest border region (2ML -5ML) show honeycomb type structures with all NCs oriented with the $\langle 111 \rangle$ axis upwards, as indicated by the SAED. (c) HAAFD-STEM image of a step region between a 2 ML and 3 ML silicene structure. (d) Tilting of the sample over 48 degrees shows the crystallographic necks between NCs and bond angles of 90 degrees. (e) A 3D visualization of the reconstructed volume

of a region between 3 and 4 ML, with the NCs of the bottom, second, third and fourth layers indicated by purple, green, blue and yellow colors respectively. (f) The 3 ML structure constitutes an ABC stacking, whereas the 4ML structure an ABCA stacking, in agreement with the coherent multilayered silicene geometry.

Defects in the honeycomb structure, considering the nanocrystals as atomic sites: Although the superstructures appear regular and periodic over a very large number of unit cells as shown by Fourier transform analysis (figure S6), several types of disorder can be observed. Here, we first make abstraction of the atomic structure of the nanocrystals, i.e. we consider the nanocrystals as "artificial atom sites" of a silicene structure. The most obvious "artificial atom" defects that we observe are presented in Figure 4. Fig. 4a shows a missing NC in the silicene structure, i.e. a vacancy. Fig. 4b shows a ring with 7 NCs (instead of the regular 6) due to incorporation of an extra NC in the silicene structure. We should remark here that similar point defects have been observed in graphene³⁶ and NC assemblies³⁷. Figure 4c shows a remarkable one-dimensional line defect that connect silicene lattices with the same crystallographic orientation, which are however shifted with respect to each other. Another example of this defect is shown in figure S7, where a part of the honeycomb lattice is shifted causing a similar line defect. The fact that the bonding configuration is possible with only NC(100)/(100)NC epitaxy, though with strain, is also proved with a ball-and-stick chemistry model (Figure S8). Also more classic grain boundaries can be observed that connect silicene domains with a different orientation as presented in Fig. 4d.

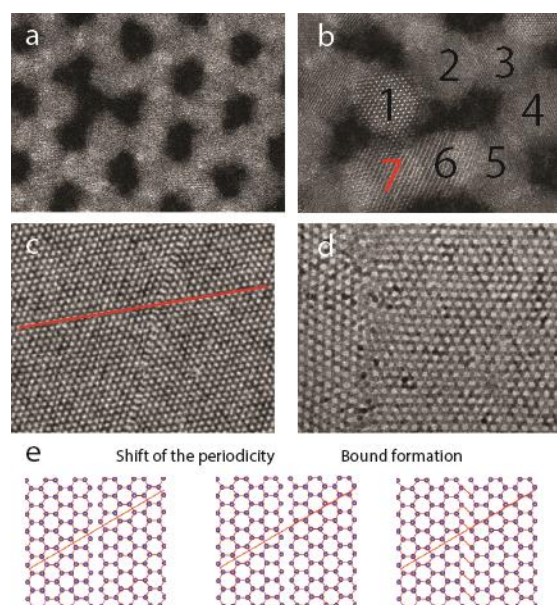


Figure 4. Overview of several types of "artificial atom (= nanocrystal)" defects in a 2D monolayer silicene lattice. (a) A missing NC in the silicene structure, i.e. vacancy, (b) an NC interstitial causes a strained 7-ring in the silicene structure. In (c) a one dimensional defect is observed and modelled in (e); the defect finds its origin in a shift of the right silicene lattice over half a unit cell with respect to the left lattice, while both lattices retain the same crystallographic orientation (see cartoon). A ball and stick model is shown in the supplementary information section, Figure S8. (d) A disordered grain boundary region between two silicene lattices that have a different crystallographic orientation.

More complex defects: Besides the zero- and one dimensional defects presented above, also more complex defects appear in the honeycomb structure with the double square and zigzag structures as prominent examples (Figure S9 a-b). Those structures often form a boundary between two silicene domains, but can also be present within one honeycomb grain. In the latter case, we could spot regions in which the honeycomb structure deviates from the hexagonal symmetry. The compressed regions with deviating geometry might be explained by NC monolayer movements along a specific direction (see Figure S7 and S9 c-f) prior to oriented attachment^{38,39,40,41}; a tentative model example is presented in Figure S10. The reason for those

relatively local NC motions could lie in local fluctuations in the solvent evaporation and suspension/air surface tension, agglomerations of capping ligands or impurities, or be the effect of sudden motions of the sample (a few tens of nanometer amplitude could be sufficient).

Disorder due to nanocrystal misalignment in the silicene lattice: We now consider each of the nanocrystal sites as an ordered array of atoms. Perfect crystallographic epitaxy should lead to an exact orientation of the nanocrystals with the [111] axis perpendicular to the plane and also completely aligned in plane. There are, however, many occasions whereby NC/NC attachment was not perfect, leading to local deviations in the alignment of the atomic lattices^{42,43}. This can be seen from high resolution images (figure 5a) and can also be deduced by the contrast difference between the attached NCs within the honeycomb lattice (figure 2c-d). To study this type of disorder, we acquired selected area electron diffraction (SAED) patterns along different tilt angles. By measuring the width of the diffraction peaks, we obtained the average angular disorder in the orientation of the NC with respect to each other. An example is shown in figure 5b, where on the left a typical SAED image of a honeycomb superstructure is shown, with six diffraction spots on the 220 ring. Azimuthal traces are made of these six spots and plotted in figure 5c in blue. These are subsequently fitted with Gaussians in red and the width of the peaks is used as a measure of the angular disorder of the NCs. This width gives the angular variation of the rotation of the $\langle 111 \rangle$ NC axis with respect to the direction perpendicular to the plane.

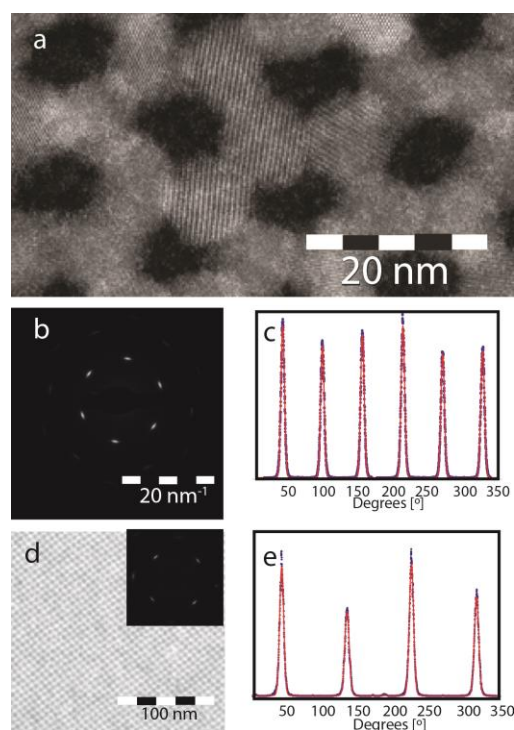


Figure 5. Analysis of NC misalignment in the silicene honeycomb lattice with SAED under two different angles. In (a) a HAADF-STEM image of a small fraction of the silicene honeycomb lattice is presented. The non-uniform crystallographic appearance indicates imperfect alignment of the NCs. (b) Typical SAED image with 6 spots on the 220 ring. (c) Plot of the spots as azimuthal traces, fitted with Gaussians. The width of the Gaussians quantify the degree of misalignment of the NCs with respect to the ideal silicene lattice. Figures d,e present a similar analysis after rotation of the sample with respect to the electron beam over 45 degrees.

The full width at half maximum of the plotted Gaussians is 3.1° . This means that 95% of the angles are within a 12.5° ($\sigma=0.4$) deviation from the ideal $\langle 110 \rangle$ direction ((111) facet pointing upwards). To test the reliability of the analysis, we measured the peak widths for a monocrystalline molybdenum crystal: 1.55° for a 95% interval ($\sigma=0.44^\circ$), averaged over 3 different locations (Figure S11). This width probably originates from a combination of instrument limitations and slight deviations from a perfect crystallographic orientation. The

broadening is much smaller compared to that of the honeycomb superlattice, which indicates that broadening of the SAED peaks is a trustful representation of the averaged orientation disorder of the NCs in the superlattice.

The analysis of the angle distribution was also performed for a 45° tilted sample orientation (see figure S12) and is presented in figures 5 d-f. In this way, the deviation of the <100> axis from that in the ideal silicene structure can be obtained, yielding an angular variation of 15.3° ($\sigma=0.73$). Notice that the <100> directions constitute the directions of NC(100)/(100)NC epitaxy and are all slightly out of plane¹⁶. This result is in line with theoretical and experimental studies showing that the alignment of crystals is energetically favorable within a 15° angle^{44,45}. The values of the angular distribution along the <100> direction are larger compared to those around the ideal <111> direction. This is expected, since the attachment process is the source of the disorder. The distribution in the <111> direction results from positive and negative errors in the misalignment along the <100> directions, yielding a lower value.

We performed the same measurements for the vertical extended (3,4, .. NC ML) silicene lattices. The angular variation around the <110> direction is 8.8° ($\sigma=0.14$), and 12.6° ($\sigma=0.6$) along the <100> direction. Multilayer silicene superlattices thus show smaller deviations in the NC orientation, compared to the 2 ML silicene lattice. Such a decrease of the disorder with increasing number of attached layers of NCs was also observed for square lattices and cubic lattices⁴⁶.

Summary: We have shown that extremely slow solvent evaporation results in improved reproducibility and specificity regarding the formation of silicene honeycomb superlattices from PbSe NC suspensions. The uniform honeycomb domains reach dimensions in the 100 μm range.

It is also possible to prepare multilayered silicene lattices. Using HAADF-STEM tomography we show that the bilayer and multilayered silicene structures of attached PbSe nanocrystals form slices of the simple cubic superstructure. Our superstructures show a long-range honeycomb periodicity, but with several types of site defects. In principle, the superstructure domains should also be atomically coherent, but we show that atomic coherency is broken by misorientations due to non-ideal epitaxial connections between the nanocrystals.

Methods

Chemicals used.

Lead acetate trihydrate $\geq 99.99\%$ trace metals basis, 1-Octadecene technical grade, 90%, Oleic acid Technical grade, 90%, Selenium powder, -100 mesh, 99.99% trace metals basis, diphenylphosphine 98%, Trioctylphosphine technical grade, 90%, Tetrachloroethylene (anhydrous, $\geq 99\%$), Toluene anhydrous, 99.8, methanol anhydrous, 99.8%, butanol anhydrous, 99.8% all bought at Sigma aldrich

Nanocrystal synthesis. PbSe NC were synthesized via a method established earlier¹. In brief, 4.77 g $\text{Pb}(\text{C}_2\text{H}_3\text{O}_2)_2 \cdot 3\text{H}_2\text{O}$, 10.35 g oleic acid and 39.75 g Octadecene (ODE) were mixed and heated (120°C) under vacuum for 5 hours to remove water and acetate. The selenium precursor was made by dissolving 3.52 g Se power, in 0.41 diphenylphosphine and 46.59 g trioctylphosphine. The selenium precursor was inject into a heated solution of the lead precursor (180°C) under vigorous stirring. After 70 sec, the reaction was quenched via injection of 30 mL of methanol/butanol mixture (1:2). The dispersion was centrifuged and subsequently dissolved in toluene. A concentrated solution of PbSe nanocrystals (approximately $1.2 \cdot 10^{-4}$ M) was washed

with methanol in a volume ratio of 1:2. The resulting brownish solution was centrifuged until a clear white solution was visible with a black precipitation. The clear solution was decanted and the black precipitation was dissolved in toluene.

Superlattice synthesis. The honeycomb superlattice was synthesized as described in the main text. A petridish was completely filled with 6.5 mL EG. This petridish was situated in another bigger petridish containing 2 mL toluene. Subsequently, 350 μL of a diluted NCs solution (7.7×10^{-8} M) in toluene was dropcasted on top of the 6.5 mL EG and both petridishes were covered with a bigger beaker (400 mL). 16 hours later the honeycomb structure was formed on top of the EG and could be transferred to any substrate. It is important that there are no high boiling point organics are present, since that will disturb the synthesis. The whole experiment is performed in a glovebox containing <0.1 ppm O_2 and no amines or other gasses than toluene. The synthesis was successful for NCs with sizes in between 5-6.3 nm.

Vertical extended superlattice synthesis. This was performed similar as the superlattice as described above except that the concentration of the NCs were increased (3-4 times), the amount of toluene in the bigger petridish was 6 mL and the synthesis was finished after 64 hours.

FT-IR measurements were performed in a Bruker Vertex 70. A special air tight liquid cell was used, bought by International Crystal Laboratories with a path length of 0.5 mm and two KBr crystals at the back and front side to make it transparent for IR light. Spectra were recorded from 400 cm^{-1} – 7500 cm^{-1} , with a KBr beam splitter, a DLaTGS D301 detector and a mid IR source. For all measurements, tetrachloroethylene (TCE) was used as solvent.

SAED measurements were performed at a Philips Tecnai operating at 200 kV. It is essential for the reproducibility of the tilting series, that the resulting SAED peaks are approximately similar in size.

HAADF-STEM images and electron tomography series were acquired on an aberration corrected ‘cubed’ FEI Titan electron microscope operated at 300 kV. Electron tomography series were acquired manually within a tilt range from -76° to $+76^{\circ}$ and an increment of 2° , using a Fischione model 2020 single-tilt tomography holder. The reconstruction was performed using the simultaneous iterative reconstruction technique (SIRT) implemented in the ASTRA toolbox [ref: W. van Aarle et al., 2015, 157, 35-47]. The reconstructed series were segmented manually by using the AMIRA software.

AUTHOR INFORMATION

Corresponding Author

*E-mail: d.vanmaekelbergh@uu.nl.

Notes

The authors declare no competing financial interest.

ACKNOWLEDGMENT

The authors acknowledge funding from the European Commission (Grant EUSMI 731019). S.B. acknowledges funding from the European Research Council (Grant 335078 COLOURATOM).

T.A. acknowledges a postdoctoral grant from the Research Foundation Flanders (FWO). The authors acknowledge financial support from the European Commission under the Horizon 2020 Programme by means of the Grant Agreement No. 731019 EUSMI.

ABBREVIATIONS

EG, ethylene glycol; NCs, nanocrystals; SAED, selected area electron diffraction; HAADF-STEM, high-angle annular dark-field scanning transmission electron microscopy;

REFERENCES

- (1) Steckel, J. S.; Coe-Sullivan, S.; Bulović, V.; Bawendi, M. G. *Adv. Mater.* **2003**, *15* (21), 1862–1866.
- (2) Ki Bae, W.; Kwak, J.; Lim, J.; Lee, D.; Ki Nam, M.; Char, K.; Lee, C.; Lee, S. *Nano Lett.* **2010**, *10* (7), 2368–2373.
- (3) Wang, J. J.; Wang, Y. Q.; Cao, F. F.; Guo, Y. G.; Wan, L. J. *J. Am. Chem. Soc.* **2010**, *132* (35), 12218–12221.
- (4) Zhang, J.; Gao, J.; Church, C. P.; Miller, E. M.; Luther, J. M.; Klimov, V. I.; Beard, M. C. *Nano Lett.* **2014**, *14* (10), 6010–6015.
- (5) Liu, Y.; Gibbs, M.; Perkins, C. L.; Tolentino, J.; Zarghami, M. H.; Bustamante, J.; Law, M. *Nano Lett.* **2011**, *11* (12), 5349–5355.
- (6) Zhitomirsky, D.; Furukawa, M.; Tang, J.; Stadler, P.; Hoogland, S.; Voznyy, O.; Liu, H.; Sargent, E. H. *Adv. Mater.* **2012**, *24* (46), 6181–6185.

- (7) Nag, A.; Kovalenko, M. V.; Lee, J.; Liu, W.; Spokoyny, B.; Talapin, D. V. *J. Am. Chem. Soc.* **2011**, *133* (27), 10612–10620.
- (8) Zhang, H.; Jang, J.; Liu, W.; Talapin, D. V. *ACS Nano* **2014**, *8* (7), 7359–7369.
- (9) Dolzhenkov, D. S.; Zhang, H.; Jang, J.; Son, J. S.; Panthani, M. G.; Shibata, T.; Chattopadhyay, S.; Talapin, D. V. *5*, 6–10.
- (10) Liu, Y.; Tolentino, J.; Gibbs, M.; Ihly, R.; Perkins, C. L.; Liu, Y.; Crawford, N.; Hemminger, J. C.; Law, M. *Nano Lett.* **2013**, *13* (4), 1578–1587.
- (11) Oh, S. J.; Berry, N. E.; Choi, J. H.; Gauding, E. A.; Lin, H.; Paik, T.; Diroll, B. T.; Muramoto, S.; Murray, C. B.; Kagan, C. R. *Nano Lett.* **2014**, *14* (3), 1559–1566.
- (12) Evers, W. H.; Goris, B.; Bals, S.; Casavola, M.; De Graaf, J.; Roij, R. Van; Dijkstra, M.; Vanmaekelbergh, D. *Nano Lett.* **2013**, *13* (6), 2317–2323.
- (13) Baumgardner, W. J.; Whitham, K.; Hanrath, T. *Nano Lett.* **2013**, *13* (7), 3225–3231.
- (14) Walravens, W.; De Roo, J.; Drijvers, E.; Ten Brinck, S.; Solano, E.; Dendooven, J.; Detavernier, C.; Infante, I.; Hens, Z. *ACS Nano* **2016**, *10* (7), 6861–6870.
- (15) Peters, J. L.; van den Bos, K. H. W.; Van Aert, S.; Goris, B.; Bals, S.; Vanmaekelbergh, D. *Chem. Mater.* **2017**, [acs.chemmater.7b01103](https://doi.org/10.1021/acs.chemmater.7b01103).
- (16) Boneschanscher, M. P.; Evers, W. H.; Geuchies, J. J.; Altantzis, T.; Goris, B.; Rabouw, F. T.; van Rossum, S. A. P.; van der Zant, H. S. J.; Siebbeles, L. D. A.; Van Tendeloo, G.; Swart, I.; Hilhorst, J.; Petukhov, A. V.; Bals, S.; Vanmaekelbergh, D. *Science* (80-.). **2014**, *344* (6190), 1377–1380.

- (17) Sarkar, S.; Acharya, S.; Chakraborty, A.; Pradhan, N. *J. Phys. Chem. Lett.* **2013**, *4* (19), 3292–3297.
- (18) O’Sullivan, C.; Gunning, R. D.; Sanyal, A.; Barrett, C. a.; Geaney, H.; Laffir, F. R.; Ahmed, S.; Ryan, K. M. *J. Am. Chem. Soc.* **2009**, *131* (34), 12250–12257.
- (19) Yu, M.; Draskovic, T. I.; Wu, Y. *Inorg. Chem.* **2014**, *53* (11), 5845–5851.
- (20) Whitham, K.; Yang, J.; Savitzky, B. H.; Kourkoutis, L. F.; Wise, F.; Hanrath, T. *Nat. Mater.* **2016**, *15* (February), 1–8.
- (21) Delerue, C. *Phys. Chem. Chem. Phys.* **2014**, *16* (47), 25734–25740.
- (22) Delerue, C.; Vanmaekelbergh, D. *2D Mater.* **2015**, *2* (3), 34008.
- (23) Kalesaki, E.; Delerue, C.; Morais Smith, C.; Beugeling, W.; Allan, G.; Vanmaekelbergh, D. *Phys. Rev. X* **2014**, *4*, 1–12.
- (24) Kalesaki, E.; Evers, W. H.; Allan, G.; Vanmaekelbergh, D.; Delerue, C. *Phys. Rev. B* **2013**, *88* (11), 115431.
- (25) Anderson, N. C.; Hendricks, M. P.; Choi, J. J.; Owen, J. S. *J. Am. Chem. Soc.* **2013**, *135* (49), 18536–18548.
- (26) Park, J.; Zheng, H.; Lee, W. C.; Geissler, P. L.; Rabani, E.; Alivisatos, A. P. *ACS Nano* **2012**, *6* (3), 2078–2085.
- (27) Lee, W. C.; Kim, B. H.; Choi, S.; Takeuchi, S.; Park, J. *J. Phys. Chem. Lett.* **2017**, *8* (3), 647–654.

- (28) Rabani, E.; Reichman, D. R.; Geissler, P. L.; Brus, L. E. *Nature* **2003**, *213901* (2002), 2–5.
- (29) Deegan, R. D.; Bakajin, O.; Dupont, T. F.; Huber, G.; Nagel, S. R.; Witten, T. a. *Nature* **1997**, *389* (6653), 827–829.
- (30) Deegan, R. D. *Phys. Rev.* **2000**, *62* (1), 756.
- (31) Hu, H.; Larson, R. G. *J. Phys. Chem. B* **2006**, *110* (14), 7090–7094.
- (32) Narayanan, S.; Wang, J.; Lin, X. M. *Phys. Rev. Lett.* **2004**, *93* (13), 1–4.
- (33) Ohara, P. C.; James R. Heath; Gelbart, W. M. *ange* **1997**, *36* (10), 1077–1080.
- (34) Yosef, G.; Rabani, E. *J. Phys. Chem. B* **2006**, *110* (42), 20965–20972.
- (35) Witten, T. A.; Sander, L. M. *Phys. Rev. Lett.* **1981**, *47* (19).
- (36) Ijäs, M.; Ervasti, M.; Uppstu, A.; Liljeroth, P.; Van Der Lit, J.; Swart, I.; Harju, A. *Phys. Rev. B - Condens. Matter Mater. Phys.* **2013**, *88* (7), 1–13.
- (37) Bodnarchuk, M. I.; Shevchenko, E. V.; Talapin, D. V. *J. Am. Chem. Soc.* **2011**, *133* (51), 20837–20849.
- (38) Geuchies, J. J.; Overbeek, C. Van; Evers, W. H.; Goris, B.; Backer, A. De; Anjan, G. P.; Rabouw, F. T.; Hilhorst, J.; Peters, J. L.; Konovalov, O.; Petukhov, A. V; Dijkstra, M.; Siebbeles, L. D. A.; Aert, S. Van; Bals, S.; Vanmaekelbergh, D. *Nat. Mater.* **2016**, *15*, 1248–1254.
- (39) Goodfellow, B. W.; Patel, R. N.; Panthani, M. G.; Korgel, B. a. **2011**, No. 100, 1–7.

- (40) Weidman, M. C.; Smilgies, D.-M.; Tisdale, W. A. *Nat. Mater.* **2016**, *15* (March), 1–8.
- (41) Bian, K.; Choi, J. J.; Kaushik, A.; Clancy, P.; Smilgies, D. M.; Hanrath, T. *ACS Nano* **2011**, *5* (4), 2815–2823.
- (42) Penn, R. L. *Science (80-.)*. **1998**, *281* (5379), 969–971.
- (43) Van Huis, M. a.; Kunneman, L. T.; Overgaag, K.; Xu, Q.; Pandraud, G.; Zandbergen, H. W.; Vanmaekelbergh, D. *Nano Lett.* **2008**, *8* (11), 3959–3963.
- (44) Fang, J.; Ding, B.; Gleiter, H. *Chem. Soc. Rev.* **2011**, *40* (11), 5347–5360.
- (45) Read, W. T.; Shockley, W. *Physical Rev. journals* **1950**, *78* (3), 275–289.
- (46) Savitzky, B. H.; Hovden, R.; Whitham, K.; Yang, J.; Wise, F.; Hanrath, T.; Kourkoutis, L. F. *Nano Lett.* **2016**, *16* (9), 5714–5718.